Arteriosclerosis, Thrombosis, and Vascular Biology

BASIC SCIENCES

FOXC1 and FOXC2 Ablation Causes Abnormal Valvular Endothelial Cell Junctions and Lymphatic Vessel Formation in Myxomatous Mitral Valve Degeneration

Can Tan, Zhi-Dong Ge, Shreya Kurup, Yaryna Dyakiv, Ting Liu, William A. Muller, Tsutomu Kume

BACKGROUND: Mitral valve (MV) disease including myxomatous degeneration is the most common form of valvular heart disease with an age-dependent frequency. Genetic evidence indicates that mutations of the human transcription factor *FOXC1* are associated with MV defects, including MV regurgitation. In this study, we sought to determine whether murine *Foxc1* and its closely related factor, *Foxc2*, are required in valvular endothelial cells (VECs) for the maintenance of MV leaflets, including VEC junctions and the stratified trilaminar ECM (extracellular matrix).

METHODS: Adult mice carrying tamoxifen-inducible, vascular endothelial cell (EC), and lymphatic EC–specific, compound *Foxc1;Foxc2* mutations (ie, EC-*Foxc*-DKO and lymphatic EC-*Foxc*-DKO mice, respectively) were used to study the function of *Foxc1* and *Foxc2* in the maintenance of MVs. The EC and lymphatic EC mutations of *Foxc1/c2* were induced at 7 to 8 weeks of age by tamoxifen treatment, and abnormalities in the MVs of these mutant mice were assessed via whole-mount immunostaining, immunohistochemistry/RNAscope, Movat pentachrome/Masson Trichrome staining, and Evans blue injection.

RESULTS: EC deletions of *Foxc1* and *Foxc2* in mice resulted in abnormally extended and thicker MVs by causing defects in the regulation of ECM organization with increased proteoglycan and decreased collagen. Notably, reticular adherens junctions were found in VECs of control MV leaflets, and these reticular structures were severely disrupted in EC-*Foxc*-DKO mice. PROX1 (prospero homeobox protein 1), a key regulator in a subset of VECs on the fibrosa side of MVs, was downregulated in EC-*Foxc1/c2* mutant VECs. Furthermore, we determined the precise location of lymphatic vessels in murine MVs, and these lymphatic vessels were aberrantly expanded and dysfunctional in EC-*Foxc1/c2* mutant MVs. Lymphatic EC deletion of *Foxc1/c2* also resulted in similar structural/ECM abnormalities as seen in EC-*Foxc1/c2* mutant MVs.

CONCLUSIONS: Our results indicate that *Foxc1* and *Foxc2* are required for maintaining the integrity of the MV, including VEC junctions, ECM organization, and lymphatic vessel formation/function to prevent myxomatous MV degeneration.

GRAPHIC ABSTRACT: A graphic abstract is available for this article.

Key Words: adherens junctions ■ endothelial cells ■ extracellular matrix ■ lymphatic vessels ■ mice ■ mitral valve

Valvular heart disease, which is commonly associated with myxomatous mitral valve (MV) degeneration, causes severe regurgitation leading to sudden cardiac arrest or sudden cardiac death. Myxomatous MV degeneration is a noninflammatory progressive alteration of the MV structure associated with MV prolapse (MVP), which is a condition characterized by the displacement of 1 or both leaflets of the MV into the left atrium during

Correspondence to: Tsutomu Kume, PhD, Department of Medicine, Feinberg Cardiovascular and Renal Research Institute, Feinberg School of Medicine, Northwestern University, 303 E Superior St, Chicago, IL 60611. Email t-kume@northwestern.edu
Supplemental Material is available at https://www.ahajournals.org/doi/suppl/10.1161/ATVBAHA.124.320316.
For Sources of Funding and Disclosures, see page 1958.

Arterioscler Thromb Vasc Biol is available at www.ahajournals.org/journal/atvb

Nonstandard Abbreviations and Acronyms

AJ	adherens junction
aL	anterior leaflet
EC	endothelial cell
ECM	extracellular matrix
FOXC	forkhead box C
HABP	hyaluronic acid–binding protein
IC	interstitial cell
LEC	lymphatic endothelial cell
LV	lymphatic vessel
MA	mitral annulus
MV	mitral valve
MVP	mitral valve prolapse
pL	posterior leaflet
PROX1	prospero homeobox protein 1
VEC	valvular endothelial cell
WM	whole-mount

Highlights

- Endothelial cell (EC)–specific deletion of *Foxc1* and *Foxc2* causes myxomatous degeneration of the mitral valve in mice.
- Expression of FOXC (forkhead box C) 1 and FOXC2 in valvular ECs is required for maintaining the reticular adherens junctions by regulating the expression of VE-cadherin and CD31 (cluster of differentiation 31). Normal reticular adherens junctions help to maintain the valvular EC barrier and ECM (extracellular matrix) composition to prevent myxomatous degeneration of the mitral valve.
- In mouse mitral valves, lymphatic vessels are localized beneath the valvular ECs at the atrial side of the leaflet. The lymphatic capillaries (L) are connected with the collecting lymphatic vessels located at the atrial side of the mitral annulus.
- In mouse mitral valves, deletion of *Foxc1* and *Foxc2* in lymphatic ECs causes abnormal formation of lymphatic vessels, which are functionally defective due to the degeneration of the lymphatic valves, therefore leading to altered ECM composition, and then resulting in myxomatous degeneration of the mitral valve.

the contraction phase of the heart.[1,2] MVP affects >7 million Americans, whereas up to 25% of individuals with MVP will develop degenerative mitral regurgitation. MVP is a heterogeneous disease, and its pathogenesis is not fully understood. Although recent genetic studies have identified causative genes associated with MVP,[3–7] little is known about the cause of defects in the MV, which leads to the progression of MVP.

Studies using mutant mouse models are critical for elucidating the mechanisms underlying MV development and disease. In mice, MV development initiates immediately after looping the heart tube that consists of myocardial (outer) and endocardial (inner) cell layers.[8] A subpopulation of endocardial endothelial cells (ECs) undergoes endothelial-to-mesenchymal transition and migrates into the cardiac jelly of the atrioventricular canal. Following the endothelial-to-mesenchymal transition, valve mesenchymal cells (ie, interstitial cells [ICs]) and valvular ECs (VECs) proliferate and produce the ECM (extracellular matrix) to promote the elongation and maturation of the valve leaflet primordia until birth. Postnatally, the MV remodels to form 3 layers of stratified ECM,[8] an elastin-rich atrialis layer, a proteoglycan-rich spongiosa layer, and a collagen-rich fibrosa layer. Recent single-cell RNA-sequencing studies demonstrated molecularly distinct populations of VECs, ICs, and other cell types.[9,10] A specific population of valve ECs on the fibrosa side of the MV leaflet specifically expresses the transcription factor *Prox1* (prospero homeobox protein 1),[9,11,12] which is a key regulator of lymphatic EC (LEC) specification/identity and is upregulated by lymph flow.[13] Importantly, structural abnormalities in the MV are often associated with dysregulated ECM. Although valve ICs are known to produce ECM components, the contribution of VECs to MV diseases such as myxomatous degeneration remains largely unknown. How VECs participate in the maintenance of MV integrity in the adult, including the stratified trilaminar ECM structure, has yet to be elucidated.

FOXC (forkhead box C) 1 and FOXC2 are closely related members of the FOX transcription factor family and have numerous essential roles in cardiovascular development, health, and disease.[14] Mutations or changes in the copy number of human *FOXC1* are associated with autosomal-dominant Axenfeld-Rieger syndrome, which is characterized by abnormalities in the eye and extraocular defects,[15] while inactivating mutations of human *FOXC2* are responsible for the autosomal-dominant syndrome lymphedema-distichiasis, which is characterized by obstructed lymph drainage in the limbs and the growth of extra eyelashes.[16] Importantly, there is genetic evidence that human *FOXC1* mutations are associated with MV defects, including MV regurgitation,[17,18] whereas a recent study shows that mice with *Foxc2* knockdown in VECs do not exhibit any MV abnormalities.[11] Although our previous studies show that both *Foxc1* and *Foxc2* are expressed in endocardial ECs in the developing mouse heart,[19–21] it remains to be elucidated whether *Foxc1* and *Foxc2* deficiency in mitral VECs impairs the maintenance of MV integrity, including VEC junctions and ECM components.

Employing EC- and LEC-specific *Foxc1/Foxc2* double-mutant (ie, EC-*Foxc*-DKO and LEC-*Foxc*-DKO) lines, respectively, we have recently demonstrated that FOXC1 and FOXC2 play cooperative roles in blood and LECs in various organs, such as the small intestine and mesentery.[22,23] In this study, our expression analyses

revealed that both genes are highly expressed in VECs of MVs in adult mice. We found that adult EC deletions of *Foxc1* and *Foxc2* lead to dysregulated ECM components, accompanied by abnormal formation of reticular adherens junctions (AJs) in VECs of MVs and reduced expression of PROX1 in a subset of VECs. Moreover, we also determined the distribution of lymphatic vasculature in MVs, and EC-*Foxc*-DKO mice exhibited expanded but dysfunctional lymphatic vessels (LVs) with degenerated lymphatic valves in MVs. LEC deletion of *Foxc1* and *Foxc2* also resulted in structural abnormalities in MVs and myxomatous degeneration.

Taken together, the results from our new studies suggest that FOXC1 and FOXC2 are essential for the maintenance of MV integrity, including proper VEC junctions, ECM organization, and LV formation/function, therefore preventing myxomatous degeneration of MVs.

MATERIALS AND METHODS

The authors declare that all supporting data are available within the article (and its Supplemental Material).

Animal Husbandry and Treatment

Foxc1$^{fl/fl}$, *Foxc2*$^{fl/fl}$, *Foxc1*$^{fl/fl}$;*Foxc2*$^{fl/fl}$,[24] *Cdh5-Cre*^{ERT2},[25] and *Vegfr3-Cre*^{ERT2}[26] mice were used. EC- or LEC-specific *Foxc1*, *Foxc2*, and compound *Foxc1;Foxc2* mutant mice were generated by crossing *Foxc*-floxed female mice (*Foxc1*$^{fl/fl}$, *Foxc2*$^{fl/fl}$, and *Foxc1*$^{fl/fl}$;*Foxc2*$^{fl/fl}$) with *Cdh5-Cre*^{ERT2};*Foxc1*$^{fl/fl}$ (EC-*Foxc1*-KO), *Cdh5-Cre*^{ERT2};*Foxc2*$^{fl/fl}$ (EC-*Foxc2*-KO), *Cdh5-Cre*^{ERT2};*Foxc1*$^{fl/fl}$;*Foxc2*$^{fl/fl}$ (EC-*Foxc*-DKO), and *Vegfr3-Cre*^{ERT2};*Foxc1*$^{fl/fl}$;*Foxc2*$^{fl/fl}$ (LEC-*Foxc*-DKO) male mice, as described previously.[22,23] For Cre recombination efficiency detection, *mTmG/+;Cdh5-Cre*^{ERT2};*Foxc1*$^{fl/fl}$;*Foxc2*$^{fl/fl}$ (mTmG/EC-*Foxc*-DKO) mice were generated by crossing mTmG (a double-fluorescent reporter) female mice (*mTmG/mTmG;Foxc1*$^{fl/fl}$;*Foxc2*$^{fl/fl}$) with EC-*Foxc*-DKO male mice. Genotyping of mice was performed by Transnetyx, Inc. To induce gene deletion of *Foxc1* and *Foxc2* in ECs, 7- to 8-weeks old male adult mice were treated with 40-mg/mL tamoxifen (Cayman Chemical, 13258) in corn oil at a dose of 150 mg/kg by oral gavage once daily for 5 consecutive days. The information about mouse lines, mouse diets, and mouse numbers used for each experiment is provided in the Major Resources Table in the Supplemental Material.

Cre Recombination Efficiency Detection

To detect Cre recombination efficiency, mTmG/EC-*Foxc*-DKO mice and their littermate control Cre-negative mTmG mice were used; 2.5 weeks after tamoxifen treatment, the hearts were harvested and fixed in 4% paraformaldehyde, followed by dehydration in 30% sucrose and being embedded in Optimal cutting temperature compound (OCT) (Sakura Finetek). Sixteen-micrometer cryosections were cut and immunostained with cluster of differentiation 31 (CD31) and green fluorescent protein (GFP) antibodies (Major Resources Table in the Supplemental Material) and a nuclear-specific dye 4′,6-diamidino-2-phenylindole (DAPI). Enhanced GFP (EGFP) signal was detected by imaging to evaluate the Cre recombination efficiency.

Tissue Collection

Four to 5 weeks after tamoxifen treatment, the hearts were collected for histological analysis. Briefly, transcardial perfusion was performed on the adult mice with cold phosphate buffer solution ([PBS]; plus 10-U/mL heparin) followed by 4% paraformaldehyde after anesthesia. The hearts were then dissected and postfixed in 4% paraformaldehyde at 4 °C for 2 to 4 hours (for frozen or whole-mount [WM] samples) or overnight (for paraffin-embedded samples). The fixed hearts were then processed to OCT- or paraffin-embedded samples. For WM staining of MVs, after the fixation of the heart, the MVs (anterior leaflets [aLs] and posterior leaflets [pLs]) together with their connected mitral annulus (MA) and papillary muscles were dissected and processed to the staining.

WM Staining

WM staining of MVs was performed as previously described[23] with slight modifications. Briefly, after fixation, the dissected MVs together with the connected MA and the papillary muscles were permeabilized in PBST (0.3% Triton X-100 in PBS) for 1 hour at 4 °C, blocked in blocking buffer (5% donkey serum, 0.5% BSA, 0.3% Triton X-100, and 0.1% NaN_3 in PBS) for 2 hours at 4 °C, and then incubated with the indicated primary antibodies (Major Resources Table in the Supplemental Material) diluted in the blocking buffer for 2 to 3 days at 4 °C. Samples were washed with PBST several times, followed by incubation with indicated fluorochrome-conjugated secondary antibodies (Major Resources Table in the Supplemental Material) diluted in the blocking buffer for 2 days at 4 °C. The samples were washed again with PBST several times, postfixed with 4% paraformaldehyde. Most of the papillary muscle was removed before the MVs were cleared with FocusClear (CelExplorer Labs, FC-101) and flat-mounted on slides in the mounting medium. A similar protocol was applied to the negative control samples, but they were incubated in the blocking buffer only, while the experimental samples were incubated in primary antibodies.

Movat Pentachrome Staining and Masson Trichrome Staining

Movat Pentachrome and Masson Trichrome staining were performed on 4-μm paraffin sections of the hearts according to the manufacturer's instructions (Scytek Laboratories, MPS2; Thermo Scientific, 87019).

Immunohistochemistry Staining

Immunohistochemistry (IHC) staining on 4-μm paraffin sections (IHC-P) and IHC staining on 10- to 16-μm frozen sections (IHC-F) were performed, as previously described.[23] The sections incubated in blocking buffer without primary antibodies were used as negative controls. The antibodies used are listed in the Major Resources Table in the Supplemental Material.

RNAscope Costained With Immunohistochemistry

Freshly cut paraffin sections (4 μm) were used for RNAscope (RNA in situ hybridization analysis) followed by immunohistochemistry staining. Briefly, RNAscope[27] was performed by using RNAscope Multiplex Fluorescent Reagent Kit v2 (Advanced

Cell Diagnostics, Inc [ACD], 323100), RNAscope mRNA probes (mouse *Prox1*: ACD 488591; *Cdh5*: ACD 312531-C3; *Pecam1*: ACD 316721; mouse positive control probe: ACD 320881, *Ubc*-C3 was selected; and negative control probe: bacteria *dapB*, ACD 320871), and tyramide conjugates (568 and 647, Thermo Fisher, B40956 and B40958) on the ACD HybEZ II Hybridization System (ACD, 321710) according to the manufacturer's instructions. After RNAscope staining, the sections were incubated with blocking buffer (5% donkey serum, 0.5% BSA, 0.3% Triton X-100, and 0.1% NaN_3 in PBS) for 1 hour at room temperature and then goat anti-CD31 antibody (R&D AF3628) in blocking buffer for overnight at 4 °C. After several washing steps with PBS, the sections were incubated in donkey anti-goat 488 antibody (Thermo Fisher, A-11055) in blocking buffer for 1 hour at room temperature, followed by washing with PBS and counterstain with 4′,6-diamidino-2-phenylindole. The sections were then mounted and ready for imaging.

Evans Blue and Dextran-FITC Permeability Assay

To test the penetration of tracers in MVs, control mice were treated with a mixture of Evans blue (Sigma, 206334-10G) and Dextran-FITC (Sigma, FD10S-100MG; molecular weight, 10 kDa) in PBS (5-μL/g body weight) at a dose of 50 mg/kg for each component by retro-orbital injection. At different time points (15, 30, and 60 minutes) after the treatment, the MVs were collected and imaged under a confocal microscope. For the detection of the permeability of the VEC barrier and the lymphatic drainage function in MVs, mice were treated with 50-mg/kg Evans blue in PBS by retro-orbital injection, and the MVs were collected at 15 and 60 minutes after the injection, respectively. Further staining and imaging were performed as mentioned in the Expanded Materials and Methods in the Supplemental Material.

Imaging

To image the MA with MV leaflets (as shown in Figure 2L), the fixed and dissected MVs together with the MA and papillary muscle structures were embedded in 1% agarose (Sigma, A9414-10G) in PBS. Images were taken from the perspective of the atrium under a stereo microscope (Nikon SMZ 745) connected to a camera from Nikon DS-Fi2 (for quantification) or the camera of Apple iPhone 12 Pro Max (for representative images). Flat-mount MV images (as shown in Figure 2C) were obtained using the same imaging system. Movat Pentachrome and Masson Trichrome staining images were acquired using an Olympus Vanox AHBT3 Research Microscope (Tokyo, Japan). WM, RNAscope, and immunohistochemistry staining images were acquired using a Nikon A1 Confocal Laser Microscope with the NIS-Elements Viewer software. Images were processed and analyzed with Adobe Photoshop, Fiji (ImageJ), and Imaris Workstation (for 3-dimensional reconstruction and video creation).

EC Isolation From Mouse Heart, RNA Extraction, and Quantitative Real-Time RT-PCR Analysis

ECs were isolated from mouse hearts as previously described[23] with slight modifications. RNA was then extracted from the ECs. Complementary DNA (cDNA) was synthesized followed by quantitative real-time reverse transcription PCR (RT-PCR) analysis. Detailed information is listed in the Expanded Materials and Methods in the Supplemental Material.

Echocardiography

Noninvasive transthoracic echocardiography was used to evaluate the MV in EC-*Foxc*-DKO and their littermate control mice (n=9 mice/group). Animals were sedated by the inhalation of 1.5% isoflurane and oxygen. After chest hair was removed with Nair, echocardiography was performed with a VisualSonics Vevo 3100 imaging system with a high-frequency transducer probe MX550S (Toronto, Canada), as previously described.[28,29] The 3-dimensional echocardiography was performed to image the MV and the entire heart. The apical 4-chamber view was used to visualize both mitral leaflets and their coaptation. MV regurgitation was recognized by either a blue color or a mixed color pattern of systolic backflow from the left ventricle to the left atrium on apical 4-chamber view color Doppler.

Quantification

Fiji (ImageJ) software was used for the measurement of length, area, number of cells, and fluorescent intensity of specific markers. Detailed information is listed in the Expanded Materials and Methods in the Supplemental Material.

Statistics

For quantification, statistical analysis was performed using GraphPad Prism 8.0 (GraphPad Software). Two-tailed *P* values were obtained by performing the Student unpaired *t* test or Mann-Whitney *U* test after the normality assumption was tested. Data were presented as mean±SEM or box and whisker plots of representative experiments from at least 3 biological replicates. $P<0.05$ was considered statistically significant.

Study Approval

All experimental protocols and procedures used in this study were approved by the Institutional Animal Care and Use Committee at Northwestern University.

RESULTS

Expression of FOXC1 and FOXC2 in the MV of the Mouse Heart

Previous histological studies demonstrate that murine *Foxc1* is expressed in the MV of the developing heart.[18,21] When evaluated via quantitative real-time RT-PCR, *Foxc1* was more highly expressed than *Foxc2* in $CD45^-/CD31^+$ cardiac ECs isolated from the adult mouse hearts ($P<0.001$; Figure 1A). Furthermore, both FOXC1 and FOXC2 proteins were detected in mitral VECs of adult mice with their expression more abundant in VECs on the ventricular (fibrosa) side of the MV leaflets, whereas FOXC1 was also highly expressed in ICs as well (Figure 1B).

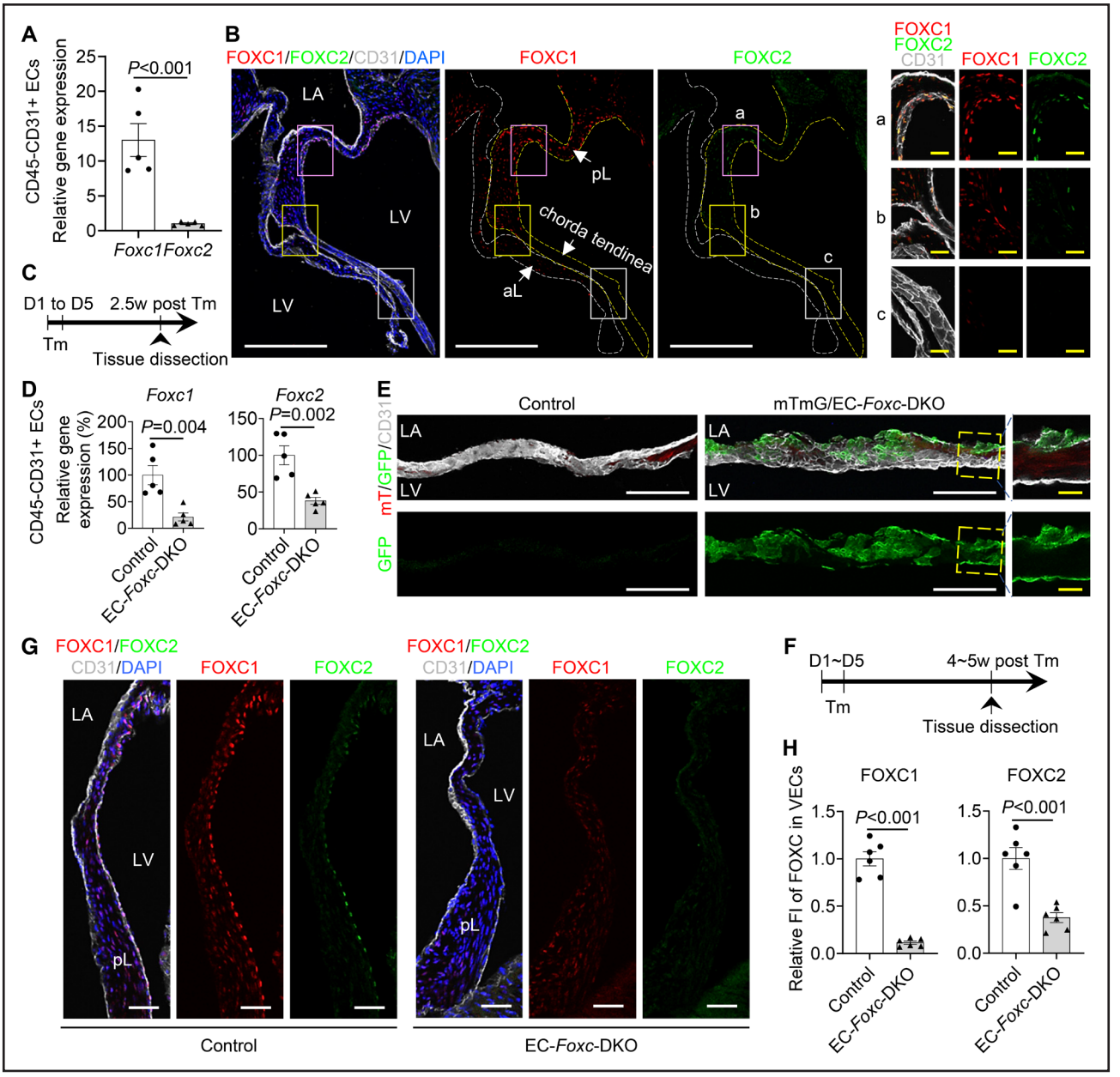

Figure 1. Expression of FOXC (forkhead box C) 1 and FOXC2 in mouse mitral valve (MV).
A, Relative mRNA expression of *Foxc1* and *Foxc2* in isolated CD45⁻CD31⁺ endothelial cells (ECs) from *Foxc1*$^{fl/fl}$;*Foxc2*$^{fl/fl}$ mouse hearts. Data are mean±SEM, Student unpaired *t* test; each symbol represents 1 mouse, N=5. **B**, Representative fluorescent images of MVs (10 µm of cryosection) from *Foxc1*$^{fl/fl}$;*Foxc2*$^{fl/fl}$ mouse stained with CD31 (cluster of differentiation 31, white), FOXC1 (red), and FOXC2 (green). White and yellow broken lines outline the anterior leaflet (aL) and posterior leaflet (pL) of the MV, respectively. Magnified images are from different regions of the pL: proximal (**a**), distal (**b**), and chorda tendinea (**c**). In MV, FOXC1-/FOXC2-expressing cells are not only ECs located on both sides (FOXC1) or fibrosa side (ventricle-facing side; FOXC2) of the MV (especially pL) but also a few interstitial cells. LA indicates left atrium; and LV, left ventricle. White/yellow scale bars, 200 or 20 µm, respectively. **C**, Schematic showing the time of tamoxifen (Tm) injection and tissue dissection for **D** and **E**. **D**, Relative mRNA expression of *Foxc1* and *Foxc2* in isolated CD45⁻CD31⁺ ECs from hearts post Tm dose in mice (control: *Foxc1*$^{fl/fl}$;*Foxc2*$^{fl/fl}$, EC-*Foxc*-DKO: *Cdh5-Cre*^{ERT2};*Foxc1*$^{fl/fl}$;*Foxc2*$^{fl/fl}$). Data are mean±SEM, Student unpaired *t* test; each symbol represents 1 mouse, N=5. **E**, Cre recombination efficiency detection in mTmG/EC-*Foxc*-DKO (*mTmG/+;Cdh5-Cre*^{ERT2};*Foxc1*$^{fl/fl}$;*Foxc2*$^{fl/fl}$) mice and littermate control mice (*mTmG/+;Foxc1*$^{fl/fl}$;*Foxc2*$^{fl/fl}$) by immunostaining of frozen heart sections with GFP (green fluorescent protein) and CD31. Representative confocal Z-stack images of these thick sections (16 µm) at low magnification and the images of optical sections with high magnification show GFP expression in ECs on both side of MV. White/yellow scale bars, 100 or 20 µm, respectively. **F**, Schematic of Tm treatment and tissue dissection for **G** and **H**. **G**, Representative confocal images of immunostaining of posterior MV leaflet sections. Scale bars, 50 µm. **H**, Quantification of fluorescent intensity (FI) of FOXC1 and FOXC2 in valvular ECs (VECs) at fibrosa side of pLs. Data are mean±SEM, Student unpaired *t* test; each symbol represents 1 mouse, N=6. DKO indicates double knock out.

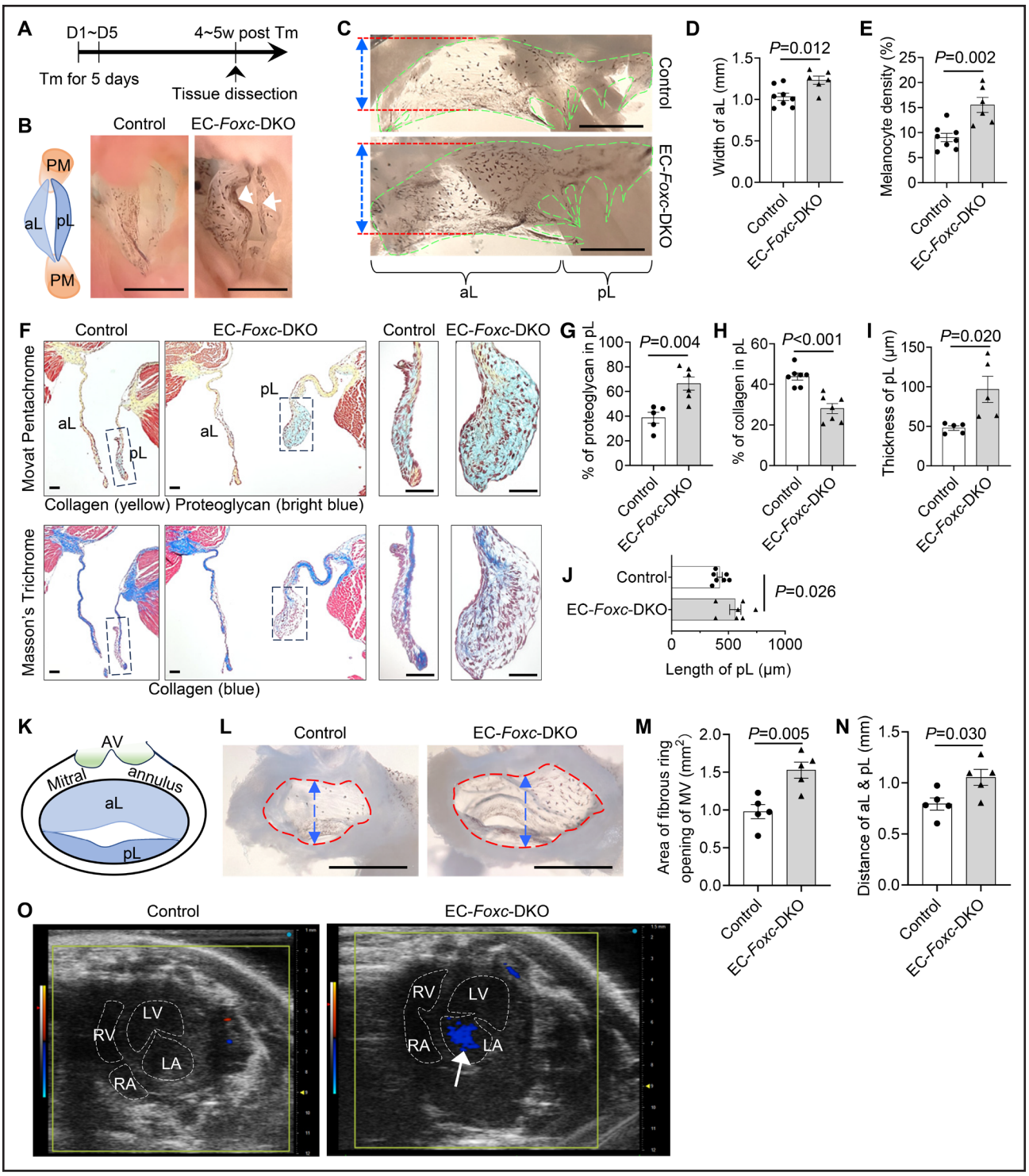

Figure 2. Endothelial cell (EC)–specific deletion of *Foxc1* and *Foxc2* leads to myxomatous degeneration of mitral valves (MVs). **A**, Schematic showing the time of tamoxifen (Tm) injection and tissue dissection for Figures 2 through 5. **B**, Representative images of MVs taken from the perspective of the left ventricle. Arrows show the accumulation of melanocytes at the free edge of the leaflets in EC-*Foxc*-DKO mice. The structural diagram in **left** shows the structures seen in **right**. PM indicates papillary muscle. Scale bar, 1 mm. **C** through **E**, Representative images (**C**) of flat-mount MVs (atrial aspect) under a stereo microscope. MVs are transparent membranes outlined by green broken lines. The darker background is the cardiac muscles at the back of the MVs. The black dots or areas on the MVs are melanocytes, which are tyrosinase positive (as shown in Figure S1A). Red lines and double-sided arrows indicate the width of the anterior leaflet (aL) of the MV. Scale bars, 1 mm. The width of aL and the density of melanocytes (%=area of melanocytes/area of MVs×100%) were quantified in **D** and **E**, respectively. Data are mean±SEM, Student unpaired *t* test; each symbol represents 1 mouse, N=6 to 8. **F** through **J**, Representative images (**F**) of Movat Pentachrome and Masson Trichrome–stained MVs in serial sections show the ECM (extracellular matrix) components including proteoglycan and collagen in MVs. Scale bars, 50 μm. The percentages of proteoglycan and collagen in posterior leaflets (pLs) (*Continued*)

Generation of Tamoxifen-Inducible, EC-Specific, *Foxc1/c2*-Mutant Mice

Because we found that both FOXC1 and FOXC2 were expressed in the mitral VECs, we analyzed tamoxifen-inducible, EC-specific, compound *Foxc1;Foxc2*-mutant (*Cdh5-Cre*^{ERT2};*Foxc1*$^{fl/fl}$;*Foxc2*$^{fl/fl}$) mice, which (after the mutation is induced in the adult) will be referred to as EC-*Foxc*-DKO mice.[22,23] To induce the mutations, adult (7–8-weeks old) mice were treated with tamoxifen (150 mg/kg) by oral gavage for 5 consecutive days, and 2.5 weeks after tamoxifen treatment (Figure 1C), quantitative real-time RT-PCR analysis confirmed that *Foxc1* and *Foxc2* expressions were significantly less common in CD45$^-$/CD31$^+$ cardiac ECs of EC-*Foxc*-DKO mice than in the corresponding cells of their control littermates (P=0.004 and 0.002; Figure 1D). Because our EC-*Foxc*-DKO mice express Cre from the EC-specific *Cdh5* promoter,[25] we crossed them with dual Rosa26mTmG reporter mice[30]; then, we treated their adult offspring with tamoxifen as described above and identified recombined EGFP$^+$ VECs in the MVs and confirmed the efficiency of Cre-mediated recombination (Figure 1E). Of note, the MVs of mTmG/EC-*Foxc*-DKO mice were abnormally shaped and much thicker than those of the control mice (see below for more details). The down-regulation of FOXC1 and FOXC2 protein in VECs (CD31$^+$) of EC-*Foxc*-DKO mice was further confirmed by immunohistochemistry staining 4 to 5 weeks after tamoxifen treatment (P<0.001; Figure 1F through 1H).

EC-Specific Deletion of *Foxc1* and *Foxc2* Impairs the Structure of MVs

We further examined structural changes in the MVs in adult EC-*Foxc*-DKO mice compared with their littermate controls 4 to 5 weeks after tamoxifen treatment (Figure 2A). Our initial investigation indicated structural abnormalities in EC-*Foxc1/c2* mutant MVs (Figure 2B), and isolated MVs of EC-*Foxc*-DKO mice were much wider (P=0.012; Figure 2C and 2D) and had an increased number of melanocytes, which were detected as black dots on MVs (P=0.002; Figure 2C and 2E) and tyrosinase positive (melanocyte marker[31] in MV; Figure S1A) compared with the control mice. Because the number of melanocytes localized in the murine MV leaflets contributes to the mechanical properties such as stiffness,[32] we next examined alterations in ECM components of the MVs of EC-*Foxc*-DKO mice via combined analyses of Movat Pentachrome and Masson Trichrome staining (Figure 2F). In male EC-*Foxc*-DKO mice, the anterior leaflets (aLs) of MVs had a slight change of ECM components (P=0.14 for proteoglycan and P=0.22 for collagen; Figure S1B and S1C), whereas the pLs had significantly altered ECM components with increased proteoglycan (P=0.004; Figure 2G) and decreased collagen (P<0.001; Figure 2H), and they were thicker and longer than the controls (P=0.020 and 0.026; Figure 2I and 2J), which suggested myxomatous degeneration of MVs. Similar structural abnormalities were found in MVs of female EC-*Foxc*-DKO mice (Figure S1D). Female mice had lighter body weights (P<0.001; Figure S1E) and smaller hearts (Figure S1F) than the male mice at 13 weeks of age, and to better quantify the differences of MVs between control and mutant groups and reduce variation, we used male mice for further studies. Milder structural abnormalities were found in MVs of either EC-*Foxc1* or *Foxc2* single KO mice (referred to as EC-*Foxc1*-KO and EC-*Foxc2*-KO mice; Figure S1G and S1H). Longer pLs (P=0.022) with decreased collagen (P=0.009) were found in EC-*Foxc1*-KO mice, whereas pLs with altered ECM components including increased proteoglycan (P=0.003) and decreased collagen (P=0.007) were found in EC-*Foxc2*-KO mice (Figure S1I through S1K) compared with their littermate controls (*Foxc1*$^{fl/fl}$ and *Foxc2*$^{fl/fl}$, respectively). Both EC-*Foxc1*-KO and EC-*Foxc2*-KO mice showed a trend toward thicker pLs compared with their controls (P=0.065 and 0.073; Figure S1L). We further examined the MA, a fibrous ring to which the MV leaflets were attached. Significantly, MA dilation was found in EC-*Foxc*-DKO mice, with an increased area of MA opening (P=0.005) and larger distance (P=0.030) across the roots of MV leaflets than in control MA (Figure 2K through 2N), which was a potential cause for mitral regurgitation that was found in 66.67% (6 of 9) of EC-*Foxc*-DKO mice at 4 weeks after tamoxifen treatment by 2-dimensional echocardiography of apical 4-chamber view (Figure 2O). Given the interactions between VECs and ICs in MV leaflets,[33] these results suggest that both *Foxc1* and *Foxc2* expressions in VECs contribute to the maintenance of the MV ECM.

Disrupted EC Junctions in the MVs of Mice With EC-Specific Deletion of *Foxc1/c2*

We next examined whether EC-*Foxc1/c2* deletions impair the maintenance of EC junctions in MVs because we and others previously found defective LEC junctions

Figure 2 Continued. were quantified in **G** and **H**. The thicknesses (**I**) and lengths (**J**) of the pLs were also measured and quantified. Data are mean±SEM, Student unpaired *t* test; each symbol represents 1 mouse, N=5 to 7. **K** through **N**, Structural diagram (**K**) showing the aL and pL, as well as the mitral annulus (MA; fibrous ring) and aortic valve (AV) presented in **L**. **L**, Representative images of the MA of MVs taken from the perspective of the atrium under a stereo microscope, showing enlargement of the MA opening in EC-*Foxc*-DKO mice 4 to 5 weeks after Tm treatment. Scale bars, 1 mm. The area of MA opening (indicated by red broken circles) and the distance across the roots of aL and pL (indicated by blue double-sided arrows) were measured and quantified in **M** and **N**, respectively. **M** and **N**, Data are mean±SEM, Student unpaired *t* test; each symbol represents 1 mouse, N=5. **O**, Images of 2-dimensional echocardiography of apical 4-chamber view show mitral regurgitation (arrow) in the heart of EC-*Foxc*-DKO mouse. DKO indicates double knock out; LA, left atrium; LV, left ventricle; RA, right atrium; and RV, right ventricle.

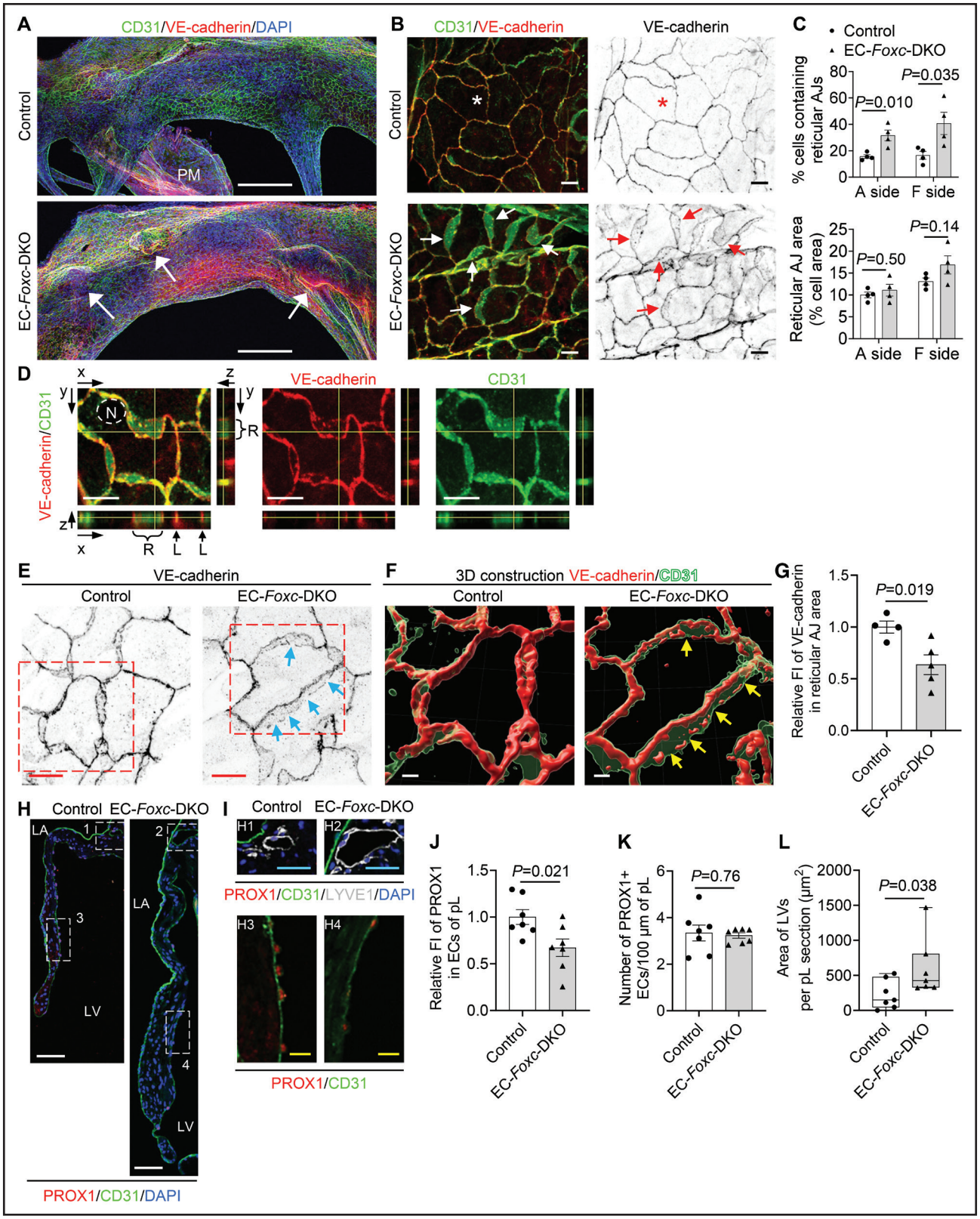

Figure 3. FOXC (forkhead box C) 1 and FOXC2 maintain the integrity of endothelial cell (EC) junctions and lymphatic vessels in the mitral valves (MVs).

A, Representative confocal images of the whole-mount posterior leaflets (pLs) of MVs stained with EC markers CD31 (cluster of differentiation 31, green) and VE-cadherin (red), as well as nuclear dye 4′,6-diamidino-2-phenylindole (DAPI; blue). Images of maximum intensity projections of the atrial aspect of pLs show thickened pL with obvious protrusions (indicated by arrows) in EC-*Foxc*-DKO mice. Note that the locally increased VE-cadherin staining in EC-*Foxc*-DKO pL is due to the images of thick pL being stacked. PM indicates papillary muscle. (*Continued*)

in the lymphatic valves of *Foxc1* and *Foxc2* mutant mice.[22,34] WM immunostaining for CD31 and VE-cadherin and confocal imaging first revealed notable protrusions in the MVs of EC-*Foxc*-DKO mice (Figure 3A, arrows), indicative of leaflet thickening and redundancy found in MVP. Remarkably, the size, shape, and arrangement of control CD31$^+$ VECs on both atrial and fibrosa sides of the pL differed in a zone-dependent manner (Figure S2A and S2B) and similar EC zones were found in the anterior leaflet. In contrast, EC-*Foxc*-DKO mice showed shortened EC zones 3 and 4 (P=0.0122 and 0.0154), as well as elongated EC zone 1 (P=0.013; Figure S2C), in which the size and number of *Foxc*-mutant VECs were smaller and increased, respectively (P=0.010 and 0.005; Figure S2D). More significantly, the reticular AJs formed at the interface of 2 overlapping VECs (Figure 3B, arrows), as previously shown in cultured ECs,[35,36] were found mainly in EC zones 3 and 4 in both control and EC-*Foxc*-DKO pLs, whereas these AJs appeared in zones 1, 2, and 5 in pLs of EC-*Foxc*-DKO mice (Figure 3B; Figure S2A). The extent of VECs containing reticular AJs was much increased in EC-*Foxc*-DKO mice (Figure 3C). The presence of the reticular AJs was further confirmed by the orthogonal view of *Z*-stack images (Figure 3D) and 3-dimensional reconstructed images (Figures 3E and 3F). It should be noted that VE-cadherin$^+$ junctions in the reticular AJs of EC-*Foxc*-DKO mice were abnormally discontinued (Figure 3F, arrows), accompanied by reduced VE-cadherin levels (P=0.019; Figure 3G; Videos S1 and S2). The formation of reticular AJs in ECs is thought to retain low permeability,[35,36] while cultured LECs under oscillatory shear stress are known to form such cellular structures to stabilize cell-cell junctions.[34] Thus, it is likely that *Foxc1/c2*-deficient VECs of MVs aberrantly form reticular AJs as a compensatory mechanism, but these cell junctions are disrupted, as seen in LECs in vivo.[22]

Furthermore, PROX1 levels in the VECs on the fibrosa side of MVs were significantly reduced in EC-*Foxc*-DKO mice (P=0.021; Figure 3H through 3J), while the number of PROX1$^+$ VECs was not altered (P=0.76; Figure 3K). Because *Prox1* acts upstream of *Foxc2* in aortic valves,[11] the downregulation of *Prox1* in *Foxc1/c2*-mutant VECs may be attributable to a feedback loop.

A combination of RNAscope (RNA in situ hybridization analysis) and immunohistochemistry staining further confirmed altered mRNA levels of specific genes expressed in VECs (Figure 4A through 4F). FOXC2 can bind to the enhancer elements upstream of both *PROX1*[37] and *CDH5*,[38] and both *Prox1* and *Cdh5*, which encode PROX1 and VE-cadherin, respectively, were decreased in VECs (immunohistochemistry-CD31$^+$) of EC-*Foxc*-DKO mice (*Prox1*; P<0.001; *Cdh5*; P=0.002; Figure 4A through 4C) due to reduced FOXC1/C2 expression in VECs (Figure 1G and 1H) compared with the controls. *Pecam1*, a gene coding for CD31 and a regulator of endothelial junctional integrity,[39] was also decreased in VECs of EC-*Foxc*-DKO mice (P<0.001; Figure 4D and 4E).

Together, these results suggest that *Foxc1/c2* expression in VECs contributes to the maintenance of the EC junctions.

Expansion of LVs in the MVs of EC-*Foxc1/c2* Mutant Mice

Limited evidence indicates that LVs are present in murine MVs,[40] while other mammalian species such as humans, pigs, and dogs have lymphatic vasculature in the MVs.[41,42] We, therefore, examined the distribution of LVs in MVs of control and EC-*Foxc*-DKO mice via coimmunostaining of the lymphatic markers, PROX1 and LYVE1 ([lymphatic vessel endothelial hyaluronan receptor 1]; Figure 3I) in paraffin sections. Careful examination revealed that in both control and EC-*Foxc*-DKO mice, most of the LVs were located at the atrial side of the root of MV leaflets (Figure 3H and 3I), where the MA area was also positioned (Figure S3A). Importantly, consistent with our previous finding that *Foxc1* and

Figure 3 Continued. Scale bars, 200 μm. **B**, Magnified confocal images of whole-mount pLs stained with CD31/VE-cadherin showing cell-cell junctions of ECs on the fibrosa side of pLs (in EC zone 5, as shown in Figure S2B). Stars indicate the linear junctions, while arrows indicate the reticular adherens junctions (AJs) of ECs. Scale bars, 10 μm. **C**, Quantification of the reticular AJs on both atrial (A) and fibrosa (F) sides of the pLs based on the images, as shown in **A**. Data are mean±SEM, Student unpaired *t* test; each symbol represents 1 mouse, N=4. **D**, Orthogonal view of Z-stack images (0.3 μm/step) showing the cell-cell junctions (stained with VE-cadherin and CD31) of endocardial ECs in pL of EC-*Foxc*-DKO mouse. Yellow lines on the stack indicate the point in the stack that is being analyzed. L indicates linear cell-cell junction; N, nucleus of EC; and R, reticular AJ area. Scale bars, 10 μm. **E** through **G**, Representative confocal images (**E**) of ECs containing reticular AJs stained with VE-cadherin in pLs of MVs. The confocal images (boxed area) were further reconstructed to 3-dimensional isosurfaces by Imaris Workstation, as shown in **F**. Arrows in **E** and **F** indicate the discontinued cell-cell junctions in the reticular AJs. Scale bars, 10 μm in **E** and 4 μm in **F**. **G**, Quantification of fluorescent intensity (FI) of VE-cadherin in reticular AJs of ECs in pLs based on the images, as shown in **E**. Data are mean±SEM, Student unpaired *t* test; each symbol represents 1 mouse, N=4 to 5. **H** through **L**, Representative fluorescent images (**H** and **I**) of pLs of MVs. Boxes 1 and 2 in **H** and their magnified images (H1 and H2) in **I** show the lymphatic vessels (LVs) located at the atrial side of the root of MVs, where the mitral annulus area is also positioned, as shown in Figure S3A, stained by lymphatic EC (LEC) markers PROX1 (prospero homeobox protein 1)/CD31/LYVE1 (lymphatic vessel endothelial hyaluronan receptor-1). Boxes 3 and 4 in **H**, as well as their magnified images (H3 and H4) in **I**, show the decreased expression of PROX1 in ECs at the fibrosa side of pL in EC-*Foxc*-DKO mouse. LA indicates left atrium; and LV, left ventricle. White/blue/yellow scale bars, 50/25/10 μm, respectively. Quantification was performed based on the fluorescent images, as shown in **H**, for relative FI of PROX1 in ECs on the fibrosa side of pL (**J**) and the number of PROX1$^+$ ECs (**K**), as well as the area of LVs in pL sections (**L**). Data are mean±SEM, Student unpaired *t* test in **J** and **K**; data are box and whisker plots, Mann-Whitney *U* test in **L**; each symbol represents 1 mouse, N=7. DKO indicates double knock out.

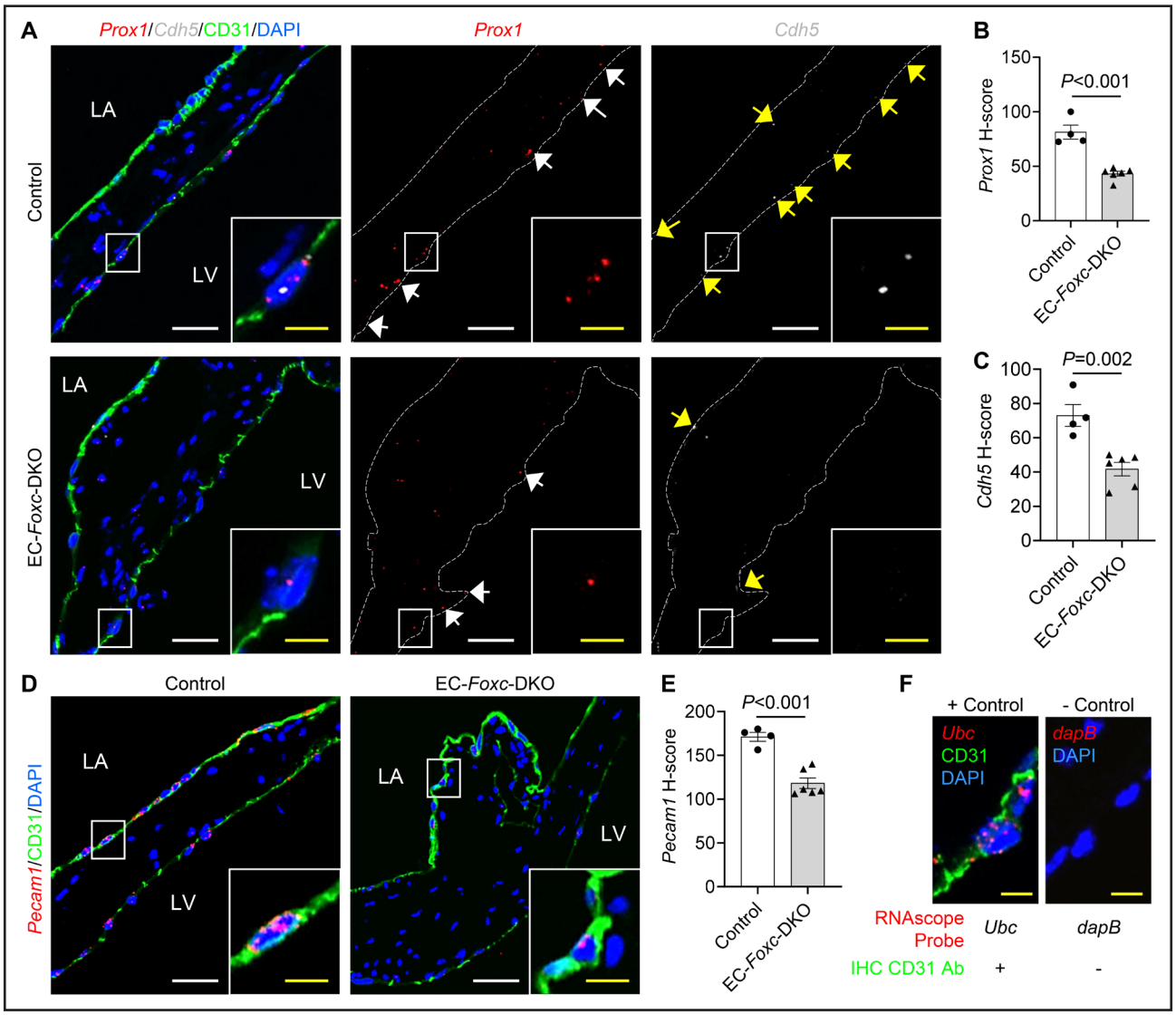

Figure 4. mRNA expression changes in valvular endothelial cells (VECs) of endothelial cell (EC)-*Foxc*-DKO mice.
A, Representative confocal images of RNAscope labeled with specific probes costained with immunohistochemistry (IHC)-CD31 (cluster of differentiation 31) in posterior leaflets show the mRNA expression of *Prox1* (white arrows) and *Cdh5* (yellow arrows) in VECs (CD31$^+$). **B** and **C**, H-score was used to quantify the mRNA expression level (see Expanded Materials and Methods) of *Prox1* (**B**) and *Cdh5* (**C**) in VECs at fibrosa side (*Prox1*) or both sides (*Cdh5*) of both anterior and posterior leaflets (aLs and pLs). **D** and **E**, Representative confocal images (**D**) and quantification of H-score (**E**) for the mRNA expression of *Pecam1* in VECs at both sides of aLs and pLs. **F**, Representative confocal images and the staining strategies for positive and negative controls were used simultaneously with the experimental samples during the RNAscope+IHC staining. *Ubc*: mouse gene encodes ubiquitin C; *dapB*: bacteria gene encodes dihydrodipicolinate reductase. White/yellow scale bars in **A**, **D**, and **F**, 20 or 5 μm, respectively. Data in (**B**), (**C**), and (**E**) are mean±SEM, Student unpaired *t* test; each symbol represents 1 mouse, N=4 to 6. DKO indicates double knock out.

Foxc2 deletion causes enhanced lymphangiogenesis,[43] EC-*Foxc*-DKO mice had dilated and higher numbers of LVs (Figure 3I and 3L; Figure S3B). Notably, in EC-*Foxc*-DKO mice, additional LVs were found in the middle of the pLs and underneath EC zone 2 where the ECs were specifically PROX1$^+$ (Figure S3C). In contrast, no blood vessels (CD31$^+$PROX1$^-$LYVE1$^-$) were found within the MV leaflets in both the control and EC-*Foxc*-DKO groups. WM immunostaining labeled with the lymphatic markers, VEGFR3 and LYVE1, as well as the EC marker CD31, further confirmed the distribution of LVs in MV leaflets (Figure 5A; Videos S3 and S4). Of note, LVs in MVs were VEGFR3$^+$ and most of the LVs were LYVE1$^+$ (Figure 5A), a marker that was also expressed in macrophages (F4/80$^+$LYVE1$^+$VEGFR3$^-$) in MVs (Figure S3D). The lymphatic capillaries extended to EC zone 2 in MVs of EC-*Foxc*-DKO mice, whereas the control mice had LVs mainly in EC zone 1 (Figure S3E; Figure 5A). No LVs were found in EC zone 3 in both groups of mice (Figure 5A). EC-*Foxc*-DKO mice had more LVs (P=0.009) with more lymphatic branching points (P=0.002) in the MV leaflets compared with the control mice (Figure 5B

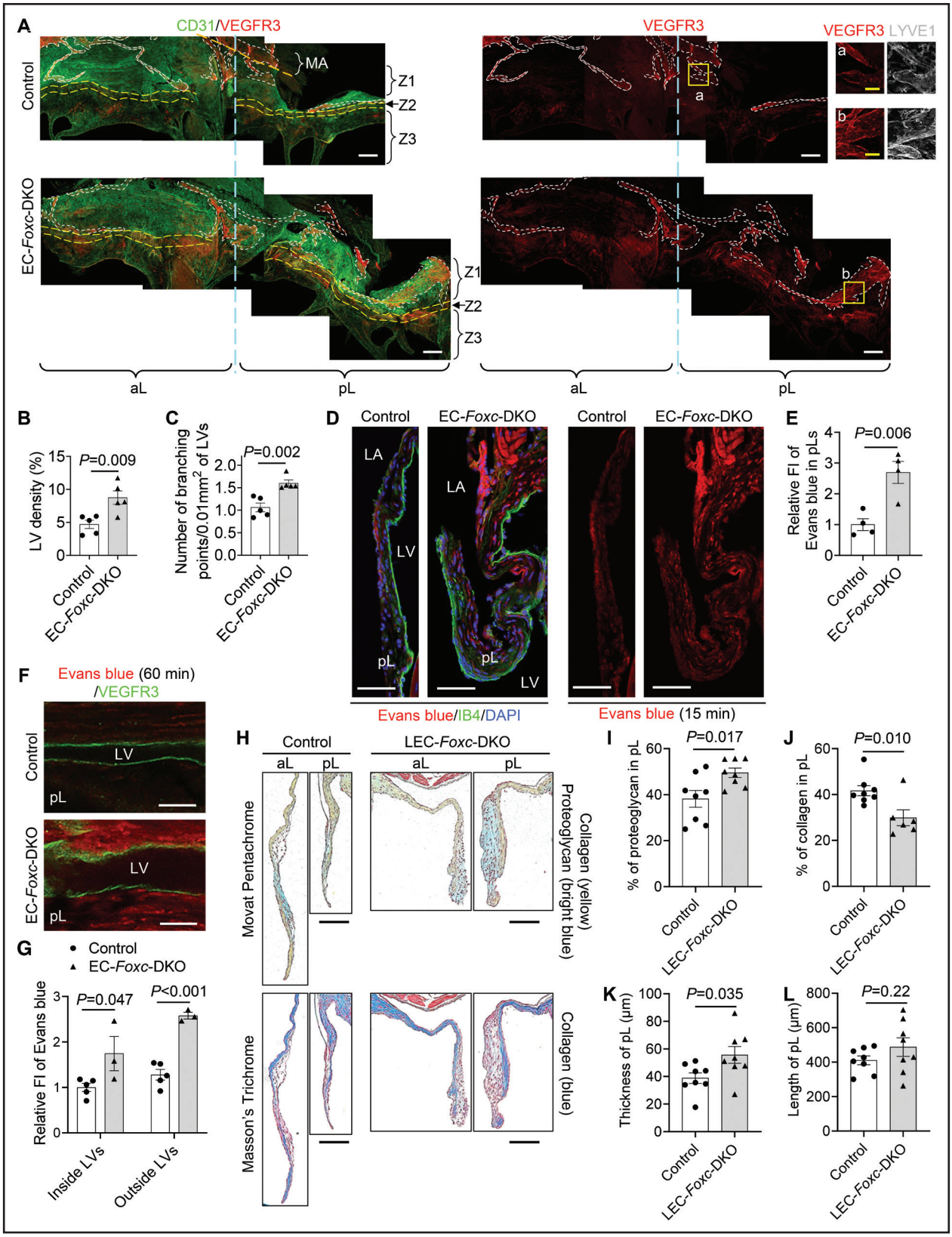

Figure 5. FOXC (forkhead box C) 1 and FOXC2 are required for the lymphatic structural and functional maintenance in mitral valves (MVs).

A, Representative confocal images of whole-mount MV leaflets (anterior leaflets [aLs] and posterior leaflets [pLs]) stained with CD31 ([cluster of differentiation 31]; green) and VEGFR3 ([vascular endothelial growth factor receptor 3]; red), as well as LYVE1 ([lymphatic vessel endothelial hyaluronan receptor-1]; white, inserts [**a**] and [**b**]). Images of maximum intensity projections of the atrial aspect (*Continued*)

 Arterioscler Thromb Vasc Biol. 2024;44:1944–1959. DOI: 10.1161/ATVBAHA.124.320316

and 5C; Videos S3 and S4). The LVs from the leaflets were connected with the LVs located in the MA (Figure S3E), which was a curved ribbon-like region that was distinguished by CD31 staining as this region was CD31 negative compared with the nearby tissue. In the control mice, LVs in the MA appeared to form lymphangions with lymphatic valves (Figure S3F), suggesting that they were collecting LVs, whereas EC-*Foxc*-DKO mice exhibited degenerated lymphatic valves in the MA, resulting in damaged lymphangion formation. Further investigation revealed that both FOXC1 (Figure S4A) and FOXC2 (Figure S4B) were expressed in LECs at the MA in control mice, but their expression was decreased in that of EC-*Foxc*-DKO mice. These data indicate that FOXC1 and FOXC2 are required for maintaining the lymphatic valve structure in MVs.

Increased VEC Permeability and Lymphatic Dysfunction in the MVs of EC-*Foxc1/c2* Mutant Mice

To examine the VEC permeability and lymphatic function in MVs, we first performed retro-orbital injection of a mixture of tracers, Evans blue dye (molecular weight, 960.81; an albumin-binding fluorescent tracer) and Dextran-FITC (molecular weight, 10 kDa), into adult mice at different time points (15, 30, and 60 minutes; Figure S5A through S5C). After the tracers entered the bloodstream following the injection, the mouse paws turned blue (Figure S5A). Because the MV leaflets have no blood vessels as described above, the tracers penetrated the MV leaflets only through the VEC barrier. Due to the different molecular sizes, the penetration rate and distribution of the tracers were different. Evans blue penetrated the interstitial regions of all EC zones of the MVs as early as 15 minutes after injection (Figure S5B), and Dextran-FITC uptaken by the F4/80$^+$ macrophages that were located in the interstitial area underneath the VECs[44] was observed mainly at EC zone 2 and sporadically at zone 1 of the MV at both 15 and 30 minutes after injection (Figure S5B and S5C). Dextran-FITC$^+$ macrophages were later found in the interstitial area at zone 3 at 30 minutes, but the number of these cells appeared to be reduced at zones 1, 2, and 3 at 60 minutes after injection (Figure S5B). These results suggest that the VEC barrier of the murine MV is permeable, and levels of the VEC permeability vary at different EC zones with zones 2 and 3 being the highest and the lowest, respectively.

Next, we sought to examine the VEC permeability and lymphatic drainage within MVs of EC-*Foxc*-DKO and control mice via the retro-orbital injection of Evans blue only because it penetrated the MVs through the VEC barrier faster and easier than Dextran-FITC. Due to the disrupted VEC junctions of the MVs in EC-*Foxc*-DKO mice (Figure 3B through 3G), increased penetration of Evans blue was detected in the MVs in EC-*Foxc*-DKO mice compared with the controls (aL: Figure S5D; pL: Figure 5D and 5E; P=0.006) at 15 minutes after injection. Notably, at 60 minutes after injection, Evans blue was less retained in the MV leaflets of the controls compared with the earlier time point (30 minutes; Figure S5B). In contrast, the dye was significantly accumulated both inside (P=0.047) and outside (P<0.001) of the LVs in the pLs of EC-*Foxc*-DKO mice at 60 minutes (Figure 5F and 5G). The impaired lymphatic drainage in the MVs was accompanied by defective lymphatic valves in the MA of EC-*Foxc*-DKO mice (Figure S3F). Together, these results suggest that EC-*Foxc*-DKO mice show the dysfunction of lymphatic drainage in the MVs.

LEC-Specific Deletion of *Foxc1* and *Foxc2* Causes Structural Abnormalities of the MV

As tamoxifen-induced Cre recombination in *Cdh5-Cre^{ERT2}* mice occurs in both VECs and LECs,[23] we further analyzed the requirements of LEC-*Foxc1/c2* expression for the integrity of the MVs in tamoxifen-inducible, LEC-specific, compound *Foxc1;Foxc2*-mutant (*Vegfr3-Cre^{ERT2};Foxc1$^{fl/fl}$;Foxc2$^{fl/fl}$*) mice (referred to as LEC-*Foxc*-DKO mice[23]). Movat Pentachrome and Masson Trichrome staining of the MVs collected 4 to 5 weeks after tamoxifen treatment were performed (Figure 5H). LEC-*Foxc*-DKO mice had thickened MV leaflets (P=0.035) with increased proteoglycan (P=0.017) and decreased collagen (P=0.010)

Figure 5 Continued. of MVs show the distribution of lymphatic vessels (LVs, outlined by white dashed lines) beneath different endothelial cell (EC) zones 1 to 3 (separated by yellow dashed lines) of the leaflets that are attached to the mitral annulus (MA). Images of optical sections with high magnification (inserts [**a**] and [**b**]) show the LVs identified by VEGFR3$^+$ and LYVE1$^+$. White/yellow scale bars, 200 or 50 μm, respectively. **B** and **C**, Quantification of LV density (**B**) and number of branching points per LV area (**C**) were performed based on the WM staining images, as shown in **A**. Data are mean±SEM, Student unpaired *t* test; each symbol represents 1 mouse, N=5. **D** and **E**, Representative confocal images (**D**) of pL sections collected at 15 minutes after Evans blue (red) injection and stained with IB4 ([isolectin B4]; green). LA indicates left atrium; and LV, left ventricle. Scale bars, 50 μm. The fluorescent intensity (FI) of Evans blue (**E**) within the pLs was quantified based on the confocal images, as shown in **D**. Data are mean±SEM, Student unpaired *t* test; each symbol represents 1 mouse, N=4. **F** and **G**, Whole-mount posterior leaflets (pLs) collected at 60 min after Evans blue (red) injection were stained with VEGFR3 (green) for the LVs. Representative confocal images (**F**) show the optical sections of the longitudinal LV segment. The FI of Evans blue inside and outside the LVs was quantified (**G**) based on the images, as shown in **F**. Data are mean±SEM, Student unpaired *t* test; each symbol represents 1 mouse, N=3 to 5. **H** through **L**, Representative images (**H**) of Movat Pentachrome and Masson Trichrome–stained MVs in serial sections show the ECM (extracellular matrix) components including proteoglycan and collagen in aLs and pLs of lymphatic EC (LEC)-*Foxc*-DKO mice and their littermate controls. Scale bars, 100 μm. Quantification for the percentages of proteoglycan (**I**) and collagen (**J**), as well as the thicknesses (**K**) and lengths (**L**) of the pLs, was performed. Data are mean±SEM, Student unpaired *t* test; each symbol represents 1 mouse, N=6 to 8. DKO indicates double knock out.

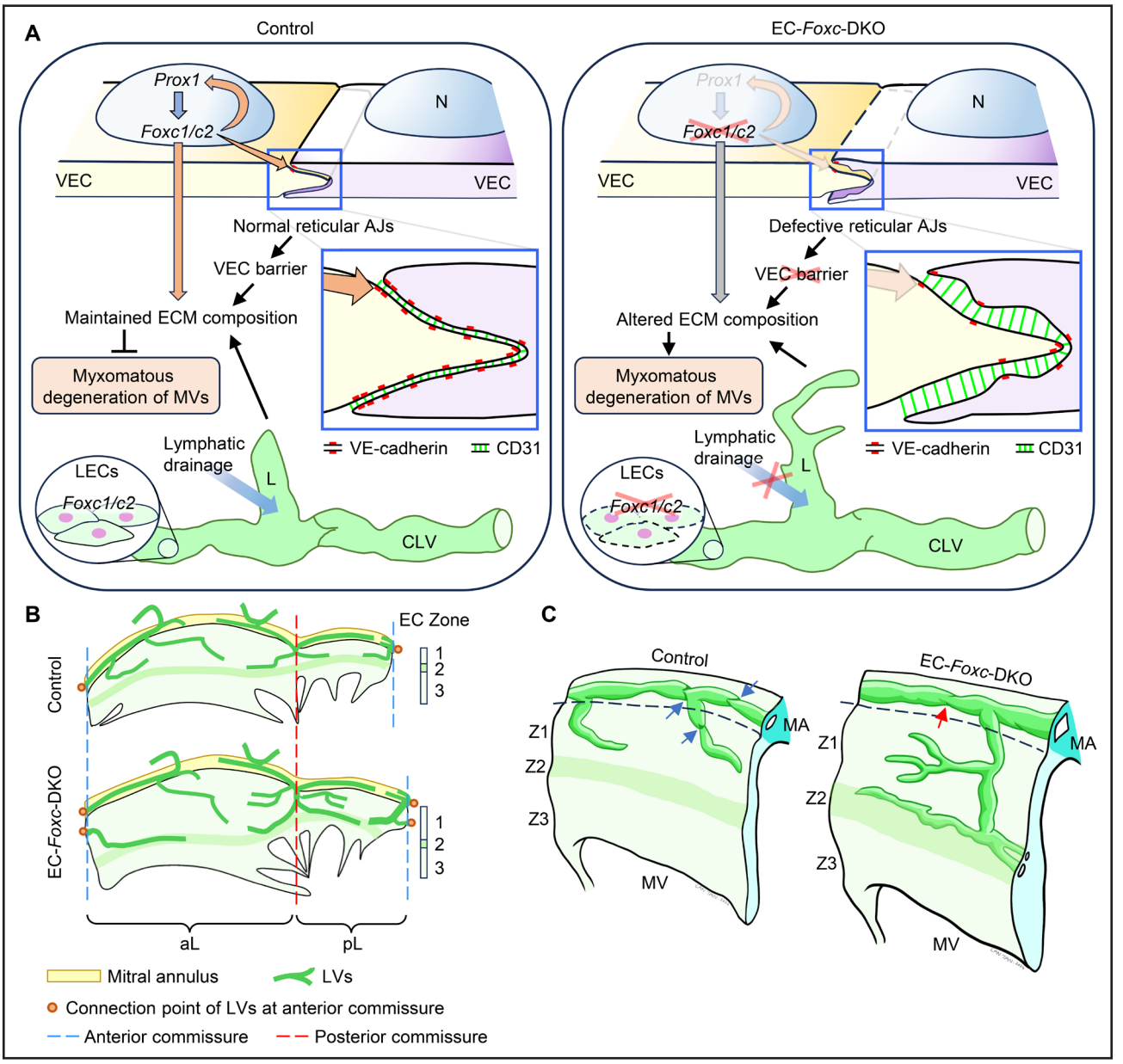

Figure 6. Mechanism of the mouse model.

A, Schematic drawing of the mechanism by which *Foxc1/c2* maintain the cell-cell junctions of valvular endothelial cells (VECs), ECM (extracellular matrix) composition, and lymphatic vessels (LVs) to prevent myxomatous degeneration of mitral valves (MVs). In normal (control) VECs, *Foxc1/c2* is regulated by *Prox1*, which can be conversely regulated by *Foxc1/c2* to maintain ECM composition via cell cross talks between VECs and valvular interstitial cells. Meanwhile, *Foxc1/c2* regulates the expression of VE-cadherin and CD31 to maintain normal reticular adherens junctions (AJs) of VECs, which also help to maintain the VEC barrier and ECM composition to prevent myxomatous degeneration of MVs. *Foxc1/Foxc2* expression in lymphatic endothelial cells (LECs) maintains the structure and function of collecting LVs (CLVs) and the blind-ended lymphatic capillaries (L), which is also important for maintaining the ECM composition. In endothelial cell (EC)-*Foxc*-DKO mice, *Foxc1/c2* ablation in VECs leads to defective reticular AJs in VECs and altered ECM composition. Deletion of *Foxc1/c2* in LECs causes structural and functional defects in LVs and causes altered ECM composition, hence resulting in myxomatous degeneration of MVs. N indicates nucleus of VEC. **B**, Structural diagram (based on whole-mount staining confocal images, as shown in Figure 5A and Figure S3E) shows the distribution of LVs in both anterior leaflet (aL) and posterior leaflet (pL) of MVs. In the control mouse, LVs start from the blind-ended capillaries underneath the lower/distal part of EC zone 1. The lymphatic capillaries are connected with the LVs located in the mitral annulus (MA) or join the LVs at the anterior/posterior commissures of the MV and then enter the MA to form collecting LVs. In EC-*Foxc*-DKO mice, the density of LVs is increased and the lymphatic capillaries extended to EC zone 2. **C**, Structural schematic shows the distribution of LVs in the interstitial area beneath the VECs at EC zones Z1 to Z3 at the atrial side of the MV leaflet. The lymphatic capillaries are connected with the collecting LVs (CLVs) located at the atrial side of the MA. Blue arrows indicate the functional lymphatic valves in control CLVs, whereas red arrow shows a degenerated and dysfunctional lymphatic valve in CLVs of EC-*Foxc*-DKO mice. DKO indicates double knock out.

compared with their littermate controls (Figure 5I through 5K), while the length of MVs was comparable to the controls (P=0.22; Figure 5L). It should be noted that the structural abnormalities of the MVs in the LEC-*Foxc*-DKO mice were milder than those in the EC-*Foxc*-DKO mice (Figure 2), indicating that the deficiency of *Foxc1/c2* in both VECs and LVs contributes to the myxomatous MV phenotypes.

Collectively, we show here that *Foxc1* and *Foxc2* are essential for the integrity of MV leaflets by maintaining VEC junctions and ECM organization, as well as LV formation and lymphatic drainage function (Figure 6A). To our knowledge, this is the first study to demonstrate reticular AJs in MVs in vivo. Our study also reveals the precise location of LVs in murine MVs (Figure 6B and 6C), which are essential for the drainage of interstitial fluid within the MVs.

DISCUSSION

Although severe MV regurgitation is life-threatening and needs surgery, the cellular and molecular mechanisms underlying its pathophysiology remain largely unknown. Here, we demonstrate that FOXC1 and FOXC2 are required for maintaining the structure of the MV, including VEC junctions, ECM organization, and LV formation. Importantly, this study demonstrates the presence of reticular AJs in MVs in vivo that play a role in the regulation of the VEC permeability and reveals the precise location of LVs in murine MVs, which are abnormally expanded and dysfunctional in EC-*Foxc*-DKO mice leading to myxomatous MV degeneration.

Although previous in vitro studies demonstrated the presence of reticular AJs in cultured ECs and their role in maintaining EC barrier function,[35,36] the pathophysiological implications of the unique EC junctions in cardiovascular disease remain to be elucidated. Remarkably, our imaging analyses reveal the disruption of the reticular AJs in the MVs of EC-*Foxc*-DKO mice (Figure 3E through 3G), accompanied by the abnormal accumulation of Evans Blue dye within the MVs (Figure 5D and 5E), suggesting increased permeability of *Foxc1/c2*-mutant VECs. Our observation accords with the previous finding that selectively disrupted reticular AJs lead to an increase in EC permeability in vitro.[35] More importantly, recent studies show that the knockdown of YAP/TAZ (Yes-associated protein/transcriptional coactivator with PDZ-binding motif) in cultured ECs results in a loss of reticular AJs and enhanced permeability,[45] and FOXC2 functionally interacts with TAZ in the junctional integrity of LECs.[34] Therefore, further studies are warranted to elucidate a unified molecular mechanism for the regulation of reticular AJs.

There is limited evidence of the presence of lymphatic vasculature in the MV of several species including humans, dogs, and pigs,[40–42] and, significantly, the precise location and morphology of LVs, as well as their function in the MV, remain unknown. In this study, we demonstrate that LVs are present in the murine MV, and they function in the drainage of interstitial fluid within the MV. Furthermore, EC deletion of *Foxc1* and *Foxc2* leads to the expansion of LVs in the MV (Figures 5A through 5C and 6B), regressed lymphatic valves (Figure S3F; Figure 6C), and defective lymphatic drainage of Evans Blue dye (Figure 5F and 5G). LEC-specific double *Foxc1/c2* mutant mice also exhibit the myxomatous MV phenotypes (Figure 5H through 5L).

Of note, because there are no LVs in EC zone 3 (free edge of the MV leaflet) and VECs in normal MVs are permeable, proteoglycans that attract water are likely to be deposited especially in this zone even in normal MVs. The accumulation of proteoglycan in the MVs of EC-*Foxc*-DKO and LEC-*Foxc*-DKO mice was more severe than the controls, as detected by Movat Pentachrome staining (Figures 2F and 5H) and WM immunostaining for HABP (hyaluronic acid–binding protein, indicative of proteoglycan deposition[46,47]; Figure S6A and S6B). Additionally, EC-*Foxc*-DKO mice had wide HABP deposition in all EC zones of MVs (Figure S6) probably due to the disrupted VEC junctions found in zones 1 to 5 (Figure 3B; Figure S2A). Overall, this is the first study to reveal the functionality of LVs in the murine MV, and further studies are needed to understand not only the development, maturation, and maintenance of the lymphatic vasculature in the MV but also its pathological growth and remodeling.

In conclusion, the findings reported here demonstrate that FOXC1 and FOXC2 are essential regulators of the maintenance of the MV via regulating VEC junctions, ECM organization, and lymphatic drainage function and advance understanding of myxomatous MV degeneration (Figure 6A).

ARTICLE INFORMATION

Received September 12, 2023; accepted June 26, 2024.

Affiliations

Department of Medicine, Feinberg Cardiovascular and Renal Research Institute (C.T., S.K., Y.D., T.L., T.K.), Departments of Pediatrics, Surgery, and Pathology, Cardiovascular-Thoracic Surgery and the Heart Center, Stanley Manne Children's Research Institute, Ann & Robert H. Lurie Children's Hospital of Chicago (Z.-D.G.), and Department of Pathology (W.A.M.), Feinberg School of Medicine, Northwestern University, Chicago, IL. Honors College, University of Illinois at Chicago (S.K.).

Acknowledgments

Cdh5-Cre^{ERT2} mice were provided by Dr Ralf Adams at the Max Planck Institute for Molecular Biomedicine, Germany. *Vegfr3-Cre*^{ERT2} mice were provided by Dr Sagrario Ortega at the Spanish National Cancer Research Center, Spain. Confocal imaging work was performed at the Northwestern University Center for Advanced Microscopy supported by NCI CCSG (National Cancer Institute, Cancer Center Support Grant) P30 CA060553 awarded to the Robert H Lurie Comprehensive Cancer Center. C. Tan contributed to conceptualization, formal analysis, investigation, methodology, project administration, supervision, validation, visualization, writing—original draft, and writing—review and editing. Z.-D. Ge contributed to formal analysis, investigation, validation, and visualization. S. Kurup, Y. Dyakiv, and T. Liu contributed to the investigation. W.A. Muller contributed to conceptualization

and methodology. T. Kume contributed to conceptualization, funding acquisition, investigation, project administration, supervision, writing—original draft, and writing—review and editing.

Sources of Funding

This study was supported by the National Institutes of Health grants RO1HL144129, R01HL159976, and R01EY034740 (to T. Kume).

Disclosures

None.

Supplemental Material

Expanded Materials and Methods[23]
Figures S1–S6
Videos S1–S4
Major Resources Table

REFERENCES

1. Levine RA, Hagege AA, Judge DP, Padala M, Dal-Bianco JP, Aikawa E, Beaudoin J, Bischoff J, Bouatia-Naji N, Bruneval P, et al; Leducq Mitral Transatlantic Network. Mitral valve disease--morphology and mechanisms. *Nat Rev Cardiol*. 2015;12:689–710. doi: 10.1038/nrcardio.2015.161
2. Pagnozzi LA, Butcher JT. Mechanotransduction mechanisms in mitral valve physiology and disease pathogenesis. *Front Cardiovasc Med*. 2017;4:83. doi: 10.3389/fcvm.2017.00083
3. Delwarde C, Capoulade R, Merot J, Le Scouarnec S, Bouatia-Naji N, Yu M, Huttin O, Selton-Suty C, Sellal JM, Piriou N, et al. Genetics and pathophysiology of mitral valve prolapse. *Front Cardiovasc Med*. 2023;10:1077788. doi: 10.3389/fcvm.2023.1077788
4. Ng CM, Cheng A, Myers LA, Martinez-Murillo F, Jie C, Bedja D, Gabrielson KL, Hausladen JM, Mecham RP, Judge DP, et al. TGF-beta-dependent pathogenesis of mitral valve prolapse in a mouse model of Marfan syndrome. *J Clin Invest*. 2004;114:1586–1592. doi: 10.1172/JCI22715
5. Roselli C, Yu M, Nauffal V, Georges A, Yang Q, Love K, Weng LC, Delling FN, Maurya SR, Schrolkamp M, et al. Genome-wide association study reveals novel genetic loci: a new polygenic risk score for mitral valve prolapse. *Eur Heart J*. 2022;43:1668–1680. doi: 10.1093/eurheartj/ehac049
6. Toomer KA, Yu M, Fulmer D, Guo L, Moore KS, Moore R, Drayton KD, Glover J, Peterson N, Ramos-Ortiz S, et al. Primary cilia defects causing mitral valve prolapse. *Sci Transl Med*. 2019;11:eaax0290. doi: 10.1126/scitranslmed.aax0290
7. Yu M, Kyryachenko S, Debette S, Amouyel P, Schott JJ, Le Tourneau T, Dina C, Norris RA, Hagege AA, Jeunemaitre X, et al. Genome-wide association meta-analysis supports genes involved in valve and cardiac development to associate with mitral valve prolapse. *Circ Genom Precis Med*. 2021;14:e003148. doi: 10.1161/CIRCGEN.120.003148
8. O'Donnell A, Yutzey KE. Mechanisms of heart valve development and disease. *Development*. 2020;147:dev183020. doi: 10.1242/dev.183020
9. Hulin A, Hortells L, Gomez-Stallons MV, O'Donnell A, Chetal K, Adam M, Lancellotti P, Oury C, Potter SS, Salomonis N, et al. Maturation of heart valve cell populations during postnatal remodeling. *Development*. 2019;146:dev173047. doi: 10.1242/dev.173047
10. Yan S, Peng Y, Lu J, Shakil S, Shi Y, Crossman DK, Johnson WH, Liu S, Rokosh DG, Lincoln J, et al. Differential requirement for DICER1 activity during the development of mitral and tricuspid valves. *J Cell Sci*. 2022;135:jcs.259783. doi: 10.1242/jcs.259783
11. Ho YC, Geng X, O'Donnell A, Ibarrola J, Fernandez-Celis A, Varshney R, Subramani K, Azartash-Namin ZJ, Kim J, Silasi R, et al. PROX1 inhibits PDGF-B expression to prevent myxomatous degeneration of heart valves. *Circ Res*. 2023;133:463–480. doi: 10.1161/CIRCRESAHA.123.323027
12. O'Donnell A, Gonzalez BA, Mukherjee S, Wilson R, Alfieri CM, Swoboda CO, Millay DP, Zorn AM, Yutzey KE. Localized Prox1 regulates aortic valve endothelial cell diversity and extracellular matrix stratification in mice. *Arterioscler Thromb Vasc Biol*. 2023;43:1478–1493. doi: 10.1161/atvbaha.123.319424
13. Ujiie N, Kume T. Mechanical forces in lymphatic vessel development: focus on transcriptional regulation. *Front Physiol*. 2022;13:1066460. doi: 10.3389/fphys.2022.1066460
14. Golson ML, Kaestner KH. Fox transcription factors: from development to disease. *Development*. 2016;143:4558–4570. doi: 10.1242/dev.112672
15. Seifi M, Walter MA. Axenfeld-Rieger syndrome. *Clin Genet*. 2018;93:1123–1130. doi: 10.1111/cge.13148
16. Fang J, Dagenais SL, Erickson RP, Arlt MF, Glynn MW, Gorski JL, Seaver LH, Glover TW. Mutations in FOXC2 (MFH-1), a forkhead family transcription factor, are responsible for the hereditary lymphedema-distichiasis syndrome. *Am J Hum Genet*. 2000;67:1382–1388. doi: 10.1086/316915
17. Gripp KW, Hopkins E, Jenny K, Thacker D, Salvin J. Cardiac anomalies in Axenfeld-Rieger syndrome due to a novel FOXC1 mutation. *Am J Med Genet A*. 2013;161:114–119. doi: 10.1002/ajmg.a.35697
18. Swiderski RE, Reiter RS, Nishimura DY, Alward WL, Kalenak JW, Searby CS, Stone EM, Sheffield VC, Lin JJ. Expression of the Mf1 gene in developing mouse hearts: implication in the development of human congenital heart defects. *Dev Dyn*. 1999;216:16–27. doi: 10.1002/(SICI)1097-0177(199909)216:1<16::AID-DVDY4>3.0.CO;2-1
19. Kume T, Jiang H, Topczewska JM, Hogan BL. The murine winged helix transcription factors, Foxc1 and Foxc2, are both required for cardiovascular development and somitogenesis. *Genes Dev*. 2001;15:2470–2482. doi: 10.1101/gad.907301
20. Seo S, Kume T. Forkhead transcription factors, Foxc1 and Foxc2, are required for the morphogenesis of the cardiac outflow tract. *Dev Biol*. 2006;296:421–436. doi: 10.1016/j.ydbio.2006.06.012
21. Winnier GE, Kume T, Deng K, Rogers R, Bundy J, Raines C, Walter MA, Hogan BL, Conway SJ. Roles for the winged helix transcription factors MF1 and MFH1 in cardiovascular development revealed by nonallelic noncomplementation of null alleles. *Dev Biol*. 1999;213:418–431. doi: 10.1006/dbio.1999.9382
22. Norden PR, Sabine A, Wang Y, Demir CS, Liu T, Petrova TV, Kume T. Shear stimulation of FOXC1 and FOXC2 differentially regulates cytoskeletal activity during lymphatic valve maturation. *Elife*. 2020;9:e53814. doi: 10.7554/eLife.53814
23. Tan C, Norden PR, Yu W, Liu T, Ujiie N, Lee SK, Yan X, Dyakiv Y, Aoto K, Ortega S, et al. Endothelial FOXC1 and FOXC2 promote intestinal regeneration after ischemia-reperfusion injury. *EMBO Rep*. 2023;24:e56030. doi: 10.15252/embr.202256030
24. Sasman A, Nassano-Miller C, Shim KS, Koo HY, Liu T, Schultz KM, Millay M, Nanano A, Kang M, Suzuki T, et al. Generation of conditional alleles for Foxc1 and Foxc2 in mice. *Genesis*. 2012;50:766–774. doi: 10.1002/dvg.22036
25. Sorensen I, Adams RH, Gossler A. DLL1-mediated Notch activation regulates endothelial identity in mouse fetal arteries. *Blood*. 2009;113:5680–5688. doi: 10.1182/blood-2008-08-174508
26. Martinez-Corral I, Stanczuk L, Frye M, Ulvmar MH, Dieguez-Hurtado R, Olmeda D, Makinen T, Ortega S. Vegfr3-CreER (T2) mouse, a new genetic tool for targeting the lymphatic system. *Angiogenesis*. 2016;19:433–445. doi: 10.1007/s10456-016-9505-x
27. Wang F, Flanagan J, Su N, Wang LC, Bui S, Nielson A, Wu X, Vo HT, Ma XJ, Luo Y. RNAscope: a novel in situ RNA analysis platform for formalin-fixed, paraffin-embedded tissues. *J Mol Diagn*. 2012;14:22–29. doi: 10.1016/j.jmoldx.2011.08.002
28. Ge ZD, Boyd RM, Lantz C, Thorp EB, Forbess JM. Cardio-omentopexy requires a cardioprotective innate immune response to promote myocardial angiogenesis in mice. *JTCVS Open*. 2022;10:222–242. doi: 10.1016/j.xjon.2022.02.027
29. Todd EA, Williams M, Kamiar A, Rasmussen MA, Shehadeh LA. Echocardiography protocol: a tool for infrequently used parameters in mice. *Front Cardiovasc Med*. 2022;9:1038385. doi: 10.3389/fcvm.2022.1038385
30. Muzumdar MD, Tasic B, Miyamichi K, Li L, Luo L. A global double-fluorescent Cre reporter mouse. *Genesis*. 2007;45:593–605. doi: 10.1002/dvg.20335
31. Hutcheson JD, Schlotter F, Creager MD, Li X, Pham T, Vyas P, Higashi H, Body SC, Aikawa M, Singh SA, et al. Elastogenesis correlates with pigment production in murine aortic valve leaflets. *Front Cardiovasc Med*. 2021;8:678401. doi: 10.3389/fcvm.2021.678401
32. Carneiro F, Kruithof BP, Balani K, Agarwal A, Gaussin V, Kos L. Relationships between melanocytes, mechanical properties and extracellular matrix composition in mouse heart valves. *J Long Term Eff Med Implants*. 2015;25:17–26. doi: 10.1615/jlongtermeffmedimplants.2015011748
33. Shapero K, Wylie-Sears J, Levine RA, Mayer JE Jr, Bischoff J. Reciprocal interactions between mitral valve endothelial and interstitial cells reduce endothelial-to-mesenchymal transition and myofibroblastic activation. *J Mol Cell Cardiol*. 2015;80:175–185. doi: 10.1016/j.yjmcc.2015.01.006
34. Sabine A, Bovay E, Demir CS, Kimura W, Jaquet M, Agalarov Y, Zangger N, Scallan JP, Graber W, Gulpinar E, et al. FOXC2 and fluid shear stress stabilize postnatal lymphatic vasculature. *J Clin Invest*. 2015;125:3861–3877. doi: 10.1172/JCI80454
35. Fernandez-Martin L, Marcos-Ramiro B, Bigarella CL, Graupera M, Cain RJ, Reglero-Real N, Jimenez A, Cernuda-Morollon E, Correas I, Cox S, et al.

Crosstalk between reticular adherens junctions and platelet endothelial cell adhesion molecule-1 regulates endothelial barrier function. *Arterioscler Thromb Vasc Biol.* 2012;32:e90–102. doi: 10.1161/ATVBAHA.112.252080
36. Klomp JE, Shaaya M, Matsche J, Rebiai R, Aaron JS, Collins KB, Huyot V, Gonzalez AM, Muller WA, Chew TL, et al. Time-variant SRC kinase activation determines endothelial permeability response. *Cell Chem Biol.* 2019;26:1081–1094.e6. doi: 10.1016/j.chembiol.2019.04.007
37. Kazenwadel J, Betterman KL, Chong CE, Stokes PH, Lee YK, Secker GA, Agalarov Y, Demir CS, Lawrence DM, Sutton DL, et al. GATA2 is required for lymphatic vessel valve development and maintenance. *J Clin Invest.* 2015;125:2979–2994. doi: 10.1172/JCI78888
38. De Val S, Chi NC, Meadows SM, Minovitsky S, Anderson JP, Harris IS, Ehlers ML, Agarwal P, Visel A, Xu SM, et al. Combinatorial regulation of endothelial gene expression by ETS and Forkhead transcription factors. *Cell.* 2008;135:1053–1064. doi: 10.1016/j.cell.2008.10.049
39. Privratsky JR, Newman PJ. PECAM-1: regulator of endothelial junctional integrity. *Cell Tissue Res.* 2014;355:607–619. doi: 10.1007/s00441-013-1779-3
40. Poltera AA, Hochmann A, Lambert PH. A model for cardiopathy induced by Trypanosoma brucei brucei in mice. A histologic and immunopathologic study. *Am J Pathol.* 1980;99:325–352.
41. Johnson RA, Blake TM. Lymphatics of the heart. *Circulation.* 1966;33:137–142. doi: 10.1161/01.cir.33.1.137
42. Miller AJ, Pick R, Katz LN. Lymphatics of the mitral valve of the dog. Demonstration and discussion of the possible significance. *Circ Res.* 1961;9:1005–1009. doi: 10.1161/01.res.9.5.1005
43. Fatima A, Wang Y, Uchida Y, Norden P, Liu T, Culver A, Dietz WH, Culver F, Millay M, Mukouyama YS, et al. Foxc1 and Foxc2 deletion causes abnormal lymphangiogenesis and correlates with ERK hyperactivation. *J Clin Invest.* 2016;126:2437–2451. doi: 10.1172/JCI80465
44. Kim AJ, Xu N, Yutzey KE. Macrophage lineages in heart valve development and disease. *Cardiovasc Res.* 2021;117:663–673. doi: 10.1093/cvr/cvaa062
45. Neto F, Klaus-Bergmann A, Ong YT, Alt S, Vion AC, Szymborska A, Carvalho JR, Hollfinger I, Bartels-Klein E, Franco CA, et al. YAP and TAZ regulate adherens junction dynamics and endothelial cell distribution during vascular development. *Elife.* 2018;7:e31037. doi: 10.7554/eLife.31037
46. Gupta V, Barzilla JE, Mendez JS, Stephens EH, Lee EL, Collard CD, Laucirica R, Weigel PH, Grande-Allen KJ. Abundance and location of proteoglycans and hyaluronan within normal and myxomatous mitral valves. *Cardiovasc Pathol.* 2009;18:191–197. doi: 10.1016/j.carpath.2008.05.001
47. Kim AJ, Xu N, Umeyama K, Hulin A, Ponny SR, Vagnozzi RJ, Green EA, Hanson P, McManus BM, Nagashima H, et al. Deficiency of circulating monocytes ameliorates the progression of myxomatous valve degeneration in Marfan syndrome. *Circulation.* 2020;141:132–146. doi: 10.1161/CIRCULATIONAHA.119.042391